Exploration of temperature dependent thermophysical characteristics of yield exhibiting non-Newtonian fluid flow under gyrotactic microorganisms

Muhammad Sohail, Rahila Naz, Zahir Shah, et al.

View Online   Export Citation   CrossMark

ARTICLES YOU MAY BE INTERESTED IN
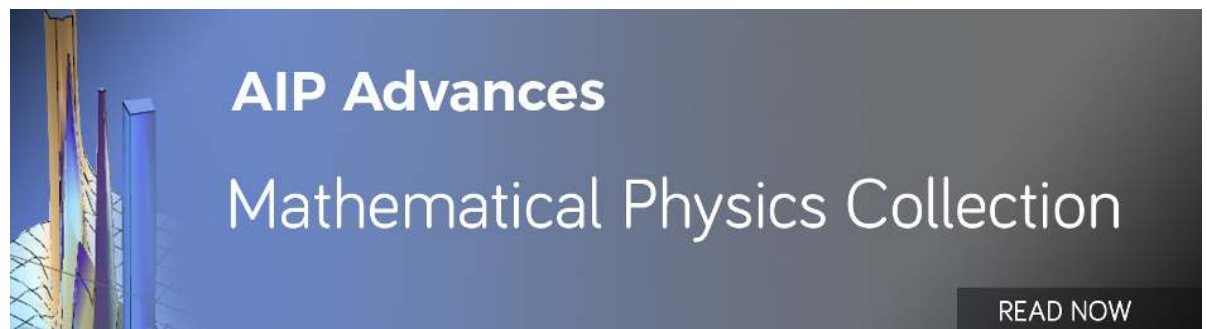
AIP Advances

Mathematical Physics Collection

READ NOW

Exploration of temperature dependent thermophysical characteristics of yield exhibiting non-Newtonian fluid flow under gyrotactic microorganisms

View Online   Export Citation   CrossMark

Muhammad Sohail,[1] (iD) Rahila Naz,[1] (iD) Zahir Shah,[2,a] (iD) Poom Kumam,[3,4,5,a] (iD) and Phatiphat Thounthong[6]

AFFILIATIONS

[1] Department of Applied Mathematics and Statistics, Institute of Space Technology, P.O. Box 2750, Islamabad 44000, Pakistan
[2] Center of Excellence in Theoretical and Computational Science (TaCS-CoE), SCL 802 Fixed Point Laboratory, Science Laboratory Building, King Mongkut's University of Technology Thonburi (KMUTT), Bangkok, Thailand
[3] KMUTT Fixed Point Research Laboratory, Room SCL 802 Fixed Point Laboratory, Science Laboratory Building, Department of Mathematics, Faculty of Science, King Mongkut's University of Technology Thonburi (KMUTT), Bangkok 10140, Thailand
[4] KMUTT-Fixed Point Theory and Applications Research Group, Theoretical and Computational Science Center (TaCS), Science Laboratory Building, Faculty of Science, King Mongkut's University of Technology Thonburi (KMUTT), Bangkok 10140, Thailand
[5] Department of Medical Research, China Medical University Hospital, China Medical University, Taichung 40402, Taiwan
[6] Renewable Energy Research Centre, Department of Teacher Training in Electrical Engineering, Faculty of Technical Education, King Mongkut's University of Technology North Bangkok, 1518 Pracharat 1 Road, Bangsue, Bangkok 10800, Thailand

[a] Authors to whom correspondence should be addressed: zahir.sha@kmutt.ac.th and poom.kum@kmutt.ac.th

ABSTRACT

Mathematical analysis of the variable thermophysical features of the three-dimensional flow of a non-Newtonian yield manifesting liquid with heat and mass transport in the presence of gyrotactic microorganisms over a nonlinear stretched surface is inspected in this exploration. The phenomenon of heat is presented in view of temperature-dependent thermal conductivity by engaging the traditional heat conduction law, whereas transport of mass is expressed by capitalizing Fick's law with temperature dependent mass diffusion. The Buongiorno model is presented for capturing the involvement of Brownian motion and thermophoresis inspirations. Additionally, the chemical reaction is considered in the mass transport expression. Boundary layer theory is applied to develop the physical problem in the form of partial differential equations. Appropriate transformation is utilized to convert the developed problem into a dimensionless system of coupled nonlinear ordinary differential equations. The transformed system is then handled analytically. The convergence analysis of the proposed scheme is presented through a table, which confirms the reliability of the suggested procedure. Moreover, the validity of the present solution and suggested scheme is presented and the limiting case of presented findings is in excellent agreement with the available literature. The computed solution of the physical variables against the influential parameters is presented through graphs. It is worth mentioning that mounting values of the fluid parameter and magnetic parameter retard the fluid flow.

I. INTRODUCTION

In last few years, the consideration of non-Newtonian fluids has achieved great attention due to its broad applications in the field of industry and engineering. Numerous fluids, including ketchup, drilling mud, paints, polymer solutions, shampoo, and so on, do not fulfill Newton's law of viscosity that represents the association between stress and strain of given fluids in a nonlinear way.

Non-Newtonian fluids with a complex nature pose a challenge to physicists, engineers, and mathematicians. In the literature, for examination of non-Newtonian fluids, numerous models have been recommended. There is no precise model containing all features of non-Newtonian fluids. The effective Maxwell model to prognosticate stress relaxation is treated as a simple viscoelastic model. The power law model is the most common existing model in the literature that has the ability to establish both shear thickening and thinning effects in non-Newtonian fluids. A Casson fluid, which is another non-Newtonian fluid, gives yield stress. If considerable shear stress is lesser than stress, then fluid behaves like a solid. When shear stress is greater than yield stress, then the fluid starts moving. A few examples of Casson fluids are honey, jelly, tomato sauce, blood, juice concentration, etc. In the available literature, the Casson fluid model was used by Aghighi et al.[1] to review the effect of the Rayleigh-Bénard convection numerically by considering a heated square cavity. Raza[2] described the characteristics of the Casson fluid flow model with slip effects and thermal radiation on magnetohydrodynamic stagnation point flow along a convected developing sheet. Ahmad et al.[3] critically interpreted the effect of chemical reaction and slip boundary conditions with mass and heat transport over a nonlinear stretching sheet of non-Newtonian fluid. The model of the Casson fluid was used to intensify the characteristics of non-Newtonian fluid. Similarly, the influence of melting heat transfer through magnetohydrodynamic (MHD) Casson fluid flow over a stretching sheet with an effect of thermal radiation in a porous medium was conferred by Mabood and Das[4] to simulate the behavior of a viscoelastic fluid in a porous regime. The Casson ferrofluid of magnetite micropolar effect over a shrinking/stretching sheet by using the Cattaneo-Christov and thermal conductivity models was scrutinized by Shah et al.[5] Mohyud-Din et al.[6] studied the squeezed flow of the Casson fluid with heat transport. Analytical solutions of the modeled physical problem are addressed via the differential transform procedure. They noticed the significant rise in temperature field by escalating the viscous dissipation parameter.

The transport of heat through the movement of microscopic electrons and the particle collision within the body is called heat conduction. This conduction law is termed "Fourier's law of heat conduction," which states that the heat transfer time rate is proportional to the negative temperature gradient and area of that gradient at right angle. Similarly, the mass transport is the net motion of mass from one region, usually phase, component, fraction, or stream, to another location. These phases occur in many mechanisms and processes, such as the biomass, food processing, solar cells, fuel cells, photovoltaic cells, photosynthesis, high capacity cooling processes, energy systems, absorption, drying, precipitation, evaporation, and membrane filtration. Due to a vast range of heat and mass transfer applications, the non-Newtonian fluid model has received much attention from many researchers.[7–12] Variable mass diffusion investigations are presented in the literature (Refs. 13–16 and 38–44), which also covered the influence of nanoparticles in the fluid flow.

In recent times, due to high costs of materials, energy, and space, researchers and scientists have introduced critical endeavors to provide more efficient heat transport equipment to bring down the cost. As a consequence, they have minimized the physical dimensions of industrial tools for a specific capability and found inventive working liquids which are the focus of observations. The effectiveness of heat transfer in fluids is highly dependent on their physical features, such as viscosity, density, and thermal conductivity. Among these, an important factor is thermal conductivity in the heat transport process. In most of the existing studies, the thermophysical characteristics of the fluids are taken to be constant. However, in general, the variable thermal conductivity of fluids employed in industry is a major constraint for heat transport properties. It is notable that the thermal conductivity may change with temperature. With this viewpoint, Nawaz et al.[17] explored viscous dissipation and Joule heating effects of MHD axisymmetric Casson fluid flow with free stream and variable thermal conductivity dependent on temperature. The swirling flow of the MHD Maxwell fluid through heat transfer with variable thermal conductivity inspiration over two coaxially rotating disks was reported by Ahmad et al.[18] Heat transfer and pressure analysis was carried out to study the effects of an axial magnetic field and temperature dependent thermal conductivity. The influence of thermal radiation and nanofluid on a Williamson fluid along a stretching cylinder in the presence of the convective boundary condition was explored by Bilal et al.[19] The variable thermal conductivity is considered during the formulation of the energy equation. Hamid and Khan[20] reported the behavior of the convective unsteady flow of a Williamson nanofluid with a magnetic effect and variable thermal conductivity in the heat transfer process. They observed that the temperature of the fluid significantly rose with increasing thermal conductivity parameter.

To interpret the magnetohydrodynamic (MHD) flow, it is relevant to study physical aspects of the MHD process. According to "Lenz's law of motion" of a conductor in a magnetic field, the magnetic field in the conductor is due to the induced electric current. When current is induced through the magnetic field by the motion of the conducting fluid, then the Lorentz force acts and changes its motion. In the MHD process, the field modifies through motion and vice versa. Recently, several researchers explored and considered the characteristics of magnetic field in their work (Refs. 21–26 and the references therein).

At present, bioconvection of nanofluids is the prime focus for several researchers. Prescribed multiphase flows consist of particles that are just carried by flow and that are not self-propelled organisms. On the other hand, the bioconvection procedure involved the suspension of the self-propelled microorganisms. This term was initiated by Platt.[27] The flow patterns were detected in the dense cultures of free-swimming microorganisms, i.e., *ciliates*, *flagellates*, and *tetrahymena*. These microorganisms resemble Bernard cells but not the existence of thermal convection. During the bioconvection process, microorganisms swam under the ground to raise up the static medium. When these microorganisms move in the flow field, their swimming positions are determined by the equilibrium state of viscous drags that result from shear stress. Gravity produced an asymmetrical diffusion of mass within the organism, and as a result, cells tend to swim to the swirling fluid segment that refers to gyrotactic mechanisms. Mosayebidorcheh et al.[28] examined the behavior of nano-bioconvection flow containing both gyrotactic microorganisms and nanoparticles by applying the method of modified least square (MLSM) that is applied on complicated types of boundary conditions. The impact of gyrotactic microorganisms on nonlinear thermal radiation and convective mass flux conditions was studied by Khan et al.[29] and Iqbal et al.[30] Nanoparticle and microorganism suspension was analyzed by Qayyum et al.,[31] which is stabilized

through bioconvection to check the surface of a rotating disk of variable thickness. Heat and mass transport exploration for the bioconvection flow around a stagnation point was reported by Usman *et al.*[32] They tackled the governing nonlinear coupled system via the wavelet procedure. They described that on augmenting the parametric values of the Brownian motion parameter, dimensionless stress increases, whereas the heat transfer coefficient diminishes.

For analytical solution, solving nonlinear equations is more difficult than solving linear ones. Generally, there are two standards for satisfactory solutions. First, it can always provide analytical approximations efficiently and, second, it can give accurate enough analytical approximations for all pertinent parameters appearing in the governing expressions along with associated conditions. By using these two standard criteria, many numerical and analytical techniques are used to solve nonlinear equations. Among these, the optimal homotopy analysis method (OHAM) is one of the most powerful tools for solving nonlinear differential equations. Mostly, OHAM is applied to boundary layer equations. Recently, the Optimal Homotopy Asymptotic Method (OHAM) was used by Marinca and Herisanu.[33] Few relevant studies concerning the OHAM are Refs. 34–47 and the references therein.

The main determination of this article is to analyze and explore thermophysical characteristics of yield exhibiting non-Newtonian fluid flow over a nonlinear stretched surface in the presence of gyrotactic microorganisms. This work is novel and different from the other work due to the consideration of variable magnetic field, temperature dependent thermal conductivity, and temperature dependent mass diffusion coefficient. The coupled system of nonlinear partial differential equations is transformed into the nonlinear system of coupled ordinary differential equations. These transformed systems of equations are solved analytically via the Optimal Homotopy Analysis Method (OHAM). The results for the given flow field, velocity, temperature, concentration, and density of motile microorganisms are analyzed graphically. These outcomes show that the fluid flow is remarkably influenced by various involved parameters. It is anticipated that the results acquired will contribute useful information on many industrial applications and also admirable previous related research works. This article is organized as follows.

Introductory discussion is given in Sec. I. Mathematical formulation is discussed in Sec. II. Some quantities of practical and engineering importance are mentioned in Sec. III. Implementation of the proposed scheme is presented with convergence in Secs. IV and V. Moreover, physical analysis is made in Sec. VI. Findings with remarks are given in Sec. VII.

II. PHYSICAL DESCRIPTION AND PROBLEM FORMULATION

Steady three-dimensional non-Newtonian bioconvection boundary layer flow past over a nonlinear stretched surface is

considered. Flow is produced due to the stretching of the bidirectional stretched surface, and it occupies the region $z \geq 0$. Variable magnetic field having strength $B(x, y) = B_{\circ}(x + y)^{\frac{n_1 - 1}{2}}$ is implemented normal to the stretched surface. It is considered that $u_1 = a(x + y)^{n_1}$, $u_2 = b(x + y)^{n_1}$, $u_3 = 0$ are the velocities along x, y, and z directions, whereas $T = T_\infty + T_{\circ}(x + y)^{n_1}$, $C = C_\infty + C_{\circ}(x + y)^{n_1}$, $m = m_\infty + m_{\circ}(x + y)^{n_1}$ are the temperature, concentration, and density of motile microorganisms at the wall. Physical quantities far away from the wall are $u_1 \to 0$, $u_2 \to 0$, $T \to T_\infty$, $C \to C_\infty$, $m \to m_\infty$. Furthermore, it is worthy to mention that transport of heat and mass is considered with temperature dependent thermal conductivity and mass diffusion coefficient. The constitutive expression for the Casson fluid model[6,12,17,34,50,51] is

$$\tau_{ab} = \left(\mu_\gamma + \frac{A_y}{(2\pi)^{\frac{1}{2}}} \right) 2e_{ab}, \quad \pi > \pi_c \ \& \ \tau_{ab} = \left(\mu_\gamma + \frac{A_y}{(2\pi_c)^{\frac{1}{2}}} \right) 2e_{ab},$$
$$\pi < \pi_c, \ \mathbf{a} = \mathbf{b} = \mathbf{1}, \ \mathbf{2}, \ \mathbf{3}, \tag{1}$$

where (μ_γ) denotes the plastic dynamic viscosity of the non-Newtonian model, (A_y) denotes the yield stress, $e_{ab} = \frac{1}{2}(\partial u_a / \partial x_b + \partial u_b / \partial x_a)$ denotes the deformation rate, (π) denotes the product of the component of the deformation rate with itself, and (π_c) denotes the critical value of this product.

Using Eq. (1) and the expression of the deformation rate, the components of tangential and normal stresses are

$$\left. \begin{array}{l} \tau_{xx} = \left(\mu_\gamma + \frac{A_y}{(2\pi)^{\frac{1}{2}}} \right) 2 \frac{\partial u_1}{\partial x}, \ \tau_{yx} = \tau_{xy} = \left(\mu_\gamma + \frac{A_y}{(2\pi)^{\frac{1}{2}}} \right) \left(\frac{\partial u_1}{\partial y} + \frac{\partial u_2}{\partial x} \right), \\[3mm] \tau_{xz} = \tau_{xz} = \left(\mu_\gamma + \frac{A_y}{(2\pi)^{\frac{1}{2}}} \right) \left(\frac{\partial u_1}{\partial y} + \frac{\partial u_2}{\partial x} \right), \ \tau_{yy} = \left(\mu_\gamma + \frac{A_y}{(2\pi)^{\frac{1}{2}}} \right) 2 \frac{\partial u_2}{\partial y}, \\[3mm] \tau_{yz} = \tau_{zy} = \left(\mu_\gamma + \frac{A_y}{(2\pi)^{\frac{1}{2}}} \right) \left(\frac{\partial u_3}{\partial y} + \frac{\partial u_2}{\partial z} \right), \ \tau_{zz} = \left(\mu_\gamma + \frac{A_y}{(2\pi)^{\frac{1}{2}}} \right) 2 \frac{\partial u_3}{\partial z}. \end{array} \right\}$$

The pertinent boundary layer equations which illustrate the physical happening shown through Fig. 1 are recorded as follows.

A. Continuity equation

The mass conservation principle is engaged which discusses the mass influx and out flux,

$$\frac{\partial u_1}{\partial x} + \frac{\partial u_2}{\partial y} + \frac{\partial u_3}{\partial z} = 0. \tag{2}$$

B. Equation of motion

The principle of force balanced is utilized in order to notice the motion of fluid particles,

$$\left. \begin{array}{l} u_1 \frac{\partial u_1}{\partial x} + u_2 \frac{\partial u_1}{\partial y} + u_3 \frac{\partial u_1}{\partial z} = \nu_a \left(1 + \frac{1}{\chi} \right) \frac{\partial^2 u_1}{\partial z^2} - \frac{\sigma}{\rho_f} B_{\circ}^2(x, y) u_1 \\[3mm] + g \left[\psi_1(T - T_\infty) + \psi_2(T - T_\infty)^2 \right] + g \left[\psi_3(C - C_\infty) + \psi_4(C - C_\infty)^2 \right], \end{array} \right\} \tag{3}$$
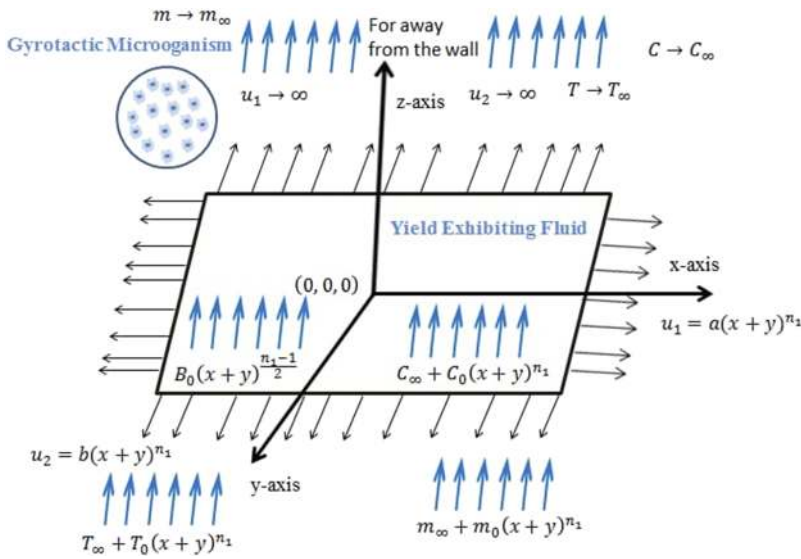
FIG. 1. Schematic representation of the present considered physical happening.

$$u_1 \frac{\partial u_2}{\partial x} + u_2 \frac{\partial u_2}{\partial y} + u_3 \frac{\partial u_2}{\partial z} = v_a \left(1 + \frac{1}{\chi}\right) \frac{\partial^2 u_2}{\partial z^2} - \frac{\sigma}{\rho_f} B_o^2(x,y) u_2. \quad (4)$$

C. Energy equation

The thermodynamics first principle is followed to derive the energy expression

$$u_1 \frac{\partial T}{\partial x} + u_2 \frac{\partial T}{\partial y} + u_3 \frac{\partial T}{\partial z} = \frac{1}{\rho_f c_p} \frac{\partial}{\partial z}\left(K_A(T) \frac{\partial T}{\partial z}\right)$$
$$+ \tau_A \left[D_B \frac{\partial C}{\partial z} \frac{\partial T}{\partial z} + \frac{D_T}{T_\infty}\left(\frac{\partial T}{\partial z}\right)^2 \right]. \quad (5)$$

D. Species equation

$$u_1 \frac{\partial C}{\partial x} + u_2 \frac{\partial C}{\partial y} + u_3 \frac{\partial C}{\partial z} = \frac{\partial}{\partial z}\left(D_A(T) \frac{\partial C}{\partial z}\right) + \frac{D_T}{T_\infty} \frac{\partial^2 T}{\partial z^2}$$
$$- K_C(C - C_\infty). \quad (6)$$

E. Gyrotactic microorganism equation

$$u_1 \frac{\partial m}{\partial x} + u_2 \frac{\partial m}{\partial y} + u_3 \frac{\partial m}{\partial z} + \gamma_a \frac{w_o}{\Delta C} \frac{\partial}{\partial z}\left(m \frac{\partial C}{\partial z}\right) = D_{m_o} \frac{\partial^2 m}{\partial z^2}. \quad (7)$$

Boundary conditions for the considered physical situation are

$$\left. \begin{array}{l} u_1 = a(x+y)^{n_1}, \ u_2 = b(x+y)^{n_1}, \ u_3 = 0, \ T = T_\infty + T_o(x+y)^{n_1}, \\ C = C_\infty + C_o(x+y)^{n_1}, \ m = m_\infty + m_o(x+y)^{n_1} \text{ at } z = 0, \\ u_1 \to 0, \ u_2 \to 0, \ T \to T_\infty, \ C \to C_\infty, \ m \to m_\infty \text{ as } z \to \infty. \end{array} \right\} \quad (8)$$

Assume the following similarity transformations:

$$\left. \begin{array}{l} u_1 = a(x+y)^{n_1} f'(\zeta), \ u_2 = a(x+y)^{n_1} g'(\zeta), \ u_3 = -\sqrt{a v_a}(x+y)^{\frac{n_1-1}{2}}\left[\frac{n_1+1}{2}(f+g) + \frac{n_1-1}{2}\zeta(f'+g')\right], \\ \zeta = \sqrt{\frac{a}{v_a}} z(x+y)^{\frac{n_1-1}{2}}, \ \theta_1(\zeta) = \frac{T-T_\infty}{T_s-T_\infty}, \ \varphi_1(\zeta) = \frac{C-C_\infty}{C_s-C_\infty}, \ N(\zeta) = \frac{m-m_\infty}{m_s-m_\infty}, \\ B(x,y) = B_o(x+y)^{\frac{n_1-1}{2}}, \ K_A(T) = K_\infty(1 + \delta_1\theta_1), \ D_A(T) = D_\infty(1 + \delta_2\theta_1). \end{array} \right\} \quad (9)$$

Equations (2)–(7) take the form

$$\left(1 + \frac{1}{\chi}\right)f''' - Mf' - n_1(f'+g')f' + \left(\frac{n_1+1}{2}\right)(f+g)f''$$
$$+ \pi_T(1 + B_T\theta_1)\theta_1 + \pi_T\tilde{N}(1 + B_C\varphi_1)\varphi_1 = 0, \quad (10)$$

$$\left(1 + \frac{1}{\chi}\right)g''' + \left(\frac{n_1+1}{2}\right)(f+g)g'' - Mg' - n_1(f'+g')g' = 0, \quad (11)$$

$$\frac{1}{Pr_\infty}(1 + \delta_1\theta_1)\theta_1'' + \frac{\delta_2}{Pr_\infty}(\theta_1')^2 + \left(\frac{n_1+1}{2}\right)(f+g)\theta_1'$$
$$+ N_T(\theta_1')^2 + N_B\theta_1'\varphi_1 = 0, \quad (12)$$

$$\frac{1}{Sc_\infty}(1 + \delta_2\theta_1)\varphi_1'' + \frac{1}{Sc_\infty}\delta_1\theta_1'\varphi_1' + \frac{N_T}{N_B}\theta_1'' + \left(\frac{n_1 + 1}{2}\right)$$
$$\times (f + g)\varphi_1' - \lambda_1\varphi_1 = 0, \tag{13}$$

$$N'' + \left(\frac{n_1 + 1}{2}\right)L_B(f + g)N' - P_E\big[N'\varphi_1 + (N + \Omega_1)\,\varphi_1\big] = 0. \tag{14}$$

The dimensionless boundary conditions[32] that manifests the flow over the strained surface are

$$\left.\begin{array}{l} f = 0,\ f' = 1,\ g = 0,\ g' = A,\ \theta_1 = 1,\ \varphi_1 = 1,\ N = 1 \text{ at } \zeta = 0, \\ f' = 0,\ \theta_1 = 0,\ \varphi_1 = 0,\ N = 0 \text{ as } \zeta \to \infty. \end{array}\right\} \tag{15}$$

III. PHYSICAL QUANTITIES OF ENGINEERING INTEREST

To discuss the fluid flow problems, skin friction coefficients $\left(\hat{C}_{fx},\ \hat{C}_{fy}\right)$ and heat transfer coefficient $\left(\hat{N}u_{xy}\right)$ are of leading curiosities. Their mathematical expressions are conferred as

$$\hat{C}_{fx} = \frac{|\tau_{zx}|_{z=0}}{\rho U_w^2},\ \hat{C}_{fy} = \frac{|\tau_{zy}|_{z=0}}{\rho V_w^2},\ \hat{N}u_{xy} = \frac{|(x + y)\,Q_w|_{z=0}}{K(T - T_\infty)}, \tag{16}$$

$$\tau_{zx} = \left(\mu_\gamma + \frac{A_y}{(2\pi)^{\frac{1}{2}}}\right)\left(\frac{\partial u_3}{\partial x} + \frac{\partial u_1}{\partial z}\right),$$
$$\tau_{zy} = \left(\mu_\gamma + \frac{A_y}{(2\pi)^{\frac{1}{2}}}\right)\left(\frac{\partial u_3}{\partial y} + \frac{\partial u_2}{\partial z}\right), \tag{17}$$

$$Q_w = -K(T)\nabla \cdot T. \tag{18}$$

Their dimensionless form is signified as

$$\hat{C}_{fx}(Re_{xy})^{\frac{1}{2}} = -\left(1 + \frac{1}{\chi}\right)f''(0),\ \hat{C}_{fy}(A)^2(Re_{xy})^{\frac{1}{2}} = -\left(1 + \frac{1}{\chi}\right)g''(0), \tag{19}$$

$$\hat{N}u_{xy}(Re_{xy})^{-\frac{1}{2}} = -\theta_1'(0)(1 + \delta_1\theta_1(0)). \tag{20}$$

In the above expressions, (u_1), (u_2), and (u_3) are velocity components in x-, y-, and z-directions, respectively, (v_a) is the kinematic viscosity of liquid, (c_p) is the specific heat, (ψ_1), (ψ_2) are the linear and nonlinear thermal expansion coefficients, (ψ_3, ψ_4) are the linear and nonlinear concentration expansion coefficients, (g) is the magnitude of gravitational acceleration, (χ) is the Casson fluid parameter, (Pr_∞) is the Prandtl number due to temperature dependent thermal conductivity, (Sc_∞) is the Schmidt number due to temperature dependent mass diffusion, (M) is Hartmann's number (magnetic parameter), (N) is the concentration of microorganisms, (π_T) is the mixed convection parameter, (τ_A) is the ratio of liquid to nanoparticle effective heat capacity, (D_B) and (D_T) are the Brownian and thermophoretic diffusing coefficients, (K_C) is the chemical reaction, (a) and (b) are the stretching rates, (n_1) is the power index, (T_S), (T_∞) and (C_S), (C_∞) are the temperature and concentration at the sheet and far away from the sheet, respectively, (L_B) is the bioconvection Lewis number, (P_E) is the Peclet number,

(λ_1) is the chemical reaction parameter, $(K_A(T))$ is the temperature dependent thermal conductivity, $(D_A(T))$ is the temperature dependent diffusion parameter, (w_o) is the maximum cell swimming speed, (δ_1), (δ_2) are the small parameters, (γ_a) is the reaction rate parameter, $(\tilde{N})$ is the ratio of concentration to thermal buoyancy forces, (N_T) is the thermophoresis parameter, (N_B) is the Brownian movement parameter, (B_T) is the nonlinear convection parameter for temperature, (B_C) is the nonlinear convection parameter for concentration, (A) is the stretching ratio parameter, (Ω_1) is the microorganism concentration difference parameter, (ρ_f) is the density of nanofluid, (ρ_p) is the density of nanoparticles, and (ρ_m) is the density of microorganism particles.

IV. OPTIMAL HOMOTOPY ANALYSIS METHOD

The optimal homotopy procedure is a powerful tool used to handle the complex nonlinear system of boundary value problems arising in applied physics and numerous engineering disciplines. To achieve the successive iterations by OHAM, we first select the initial guess and linear operator which has the characteristics that they satisfy the given boundary conditions of the considered problem. It has several advantages over many existing algorithms.

- No small or large parameter is required for it.
- No transform function and its derivatives such as Laplace, Fourier, and differential transform and reduced differential procedures are required.
- No stability criteria and discretization are required.
- It treats the linear and nonlinear problems in a similar fashion. No Adomian polynomial is required.

Therefore, initial guesses and their corresponding linear operator are listed as

$$\left.\begin{array}{l} f_\circ = 1 - \frac{1}{e^\varsigma},\ g_\circ = A\left(1 - \frac{1}{e^\varsigma}\right),\ (\theta_1)_\circ = \frac{1}{e^\varsigma},\ (\varphi_1)_\circ = \frac{1}{e^\varsigma},\ N_\circ = \frac{1}{e^\varsigma}, \\ L_1 = \left(D^3 - D\right)f,\ L_2 = \left(D^3 - D\right)g,\ L_3 = \left(D^2 - 1\right)\theta_1, \\ L_4 = \left(D^2 - 1\right)\varphi_1,\ L_5 = \left(D^2 - 1\right)N, \end{array}\right\} \tag{21}$$

and these linear operators conform to the following features:

$$\left.\begin{array}{l} L_1\big[s_1^* + s_2^* e^\varsigma + s_3^* e^{-\varsigma}\big] = 0, \\ L_2\big[s_4^* + s_5^* e^\varsigma + s_6^* e^{-\varsigma}\big] = 0, \\ L_3\big[s_7^* e^\varsigma + s_8^* e^{-\varsigma}\big] = 0, \\ L_4\big[s_9^* e^\varsigma + s_{10}^* e^{-\varsigma}\big] = 0, \\ L_5\big[s_{11}^* e^\varsigma + s_{12}^* e^{-\varsigma}\big] = 0, \end{array}\right\} \tag{22}$$

where $s_n^*(n = 1 - 12)$ are the constants which are to be determined by utilizing the given boundary conditions.

V. OPTIMAL CONJUNCTION REGULATOR PARAMETER

The nonzero auxiliary parameters in homotopic solutions standardize the convergence precinct as well as rate of preferred homotopic solutions. To take the optimal values of constraining parameters $\hbar_f$, h_g, $\hbar_{\theta_1}$, $\hbar_{\varphi_1}$, and h_N, we have smeared the perception of minimization by considering the average squared residual inaccuracies as recommended by Liao,[46]

TABLE I. Error reduction in series solution using OHAM.

r_1	$\widetilde{E_{r1}^{*f}}$	$\widetilde{E_{r1}^{*g}}$	$\widetilde{E_{r1}^{*\theta_1}}$	$\widetilde{E_{r1}^{*\phi_1}}$	$\widetilde{E_{r1}^{*N}}$
2	1.0421×10^{-2}	1.1035×10^{-2}	1.9136×10^{-2}	1.8291×10^{-2}	1.4785×10^{-2}
4	1.5307×10^{-4}	1.6103×10^{-3}	2.1928×10^{-3}	4.1827×10^{-3}	2.3792×10^{-3}
6	3.4065×10^{-6}	3.8430×10^{-4}	3.9724×10^{-4}	1.5189×10^{-3}	1.1794×10^{-3}
8	5.0521×10^{-7}	2.1036×10^{-5}	4.2395×10^{-6}	5.1827×10^{-4}	2.7362×10^{-4}
10	1.9128×10^{-7}	4.9283×10^{-6}	1.1937×10^{-7}	3.1437×10^{-4}	1.9526×10^{-5}
12	3.2501×10^{-8}	1.9102×10^{-8}	3.5691×10^{-8}	3.7834×10^{-5}	5.3972×10^{-6}
16	4.5631×10^{-9}	4.9103×10^{-9}	2.8491×10^{-9}	2.8193×10^{-6}	1.2803×10^{-6}
20	1.9704×10^{-12}	3.2017×10^{-10}	5.9275×10^{-10}	3.2759×10^{-7}	3.9275×10^{-7}
22	1.6208×10^{-13}	1.4937×10^{-12}	1.9516×10^{-10}	1.9172×10^{-8}	1.8626×10^{-7}
24	2.1935×10^{-14}	3.6927×10^{-13}	4.9315×10^{-11}	2.4827×10^{-9}	1.6385×10^{-8}
26	3.9372×10^{-15}	5.9814×10^{-14}	1.5412×10^{-11}	1.4693×10^{-10}	2.9238×10^{-9}
30	3.5731×10^{-17}	1.9104×10^{-15}	4.2691×10^{-12}	2.7105×10^{-12}	1.8273×10^{-10}

$$\hat{E}_{r_1}^{*f} = \frac{1}{d+1} \sum_{J=0}^{d} \left[G_f \left(\sum_{r^*=0}^{r_1} \hat{f}(\varsigma), \ \sum_{r^*=0}^{r_1} \hat{g}(\varsigma), \ \sum_{r^*=0}^{r_1} \hat{\theta}_1(\varsigma), \ \sum_{r^*=0}^{r_1} \hat{\varphi}_1(\varsigma) \right)_{\varsigma = J\delta\varsigma} \right]^2, \tag{23}$$

$$\hat{E}_{r_1}^{*g} = \frac{1}{d+1} \sum_{J=0}^{d} \left[G_g \left(\sum_{r^*=0}^{r_1} \hat{f}(\varsigma), \ \sum_{r^*=0}^{r_1} \hat{g}(\varsigma) \right)_{\varsigma = J\delta\varsigma} \right]^2, \tag{24}$$

$$\hat{E}_{r_1}^{*\theta_1} = \frac{1}{d+1} \sum_{J=0}^{d} \left[G_{\theta_1} \left(\sum_{r^*=0}^{r_1} \hat{f}(\varsigma), \ \sum_{r^*=0}^{r_1} \hat{g}(\varsigma), \ \sum_{r^*=0}^{r_1} \hat{\theta}_1(\varsigma), \ \sum_{r^*=0}^{r_1} \hat{\varphi}_1(\varsigma) \right)_{\varsigma J\delta\varsigma} \right]^2, \tag{25}$$

$$\hat{E}_{r_1}^{*\varphi_1} = \frac{1}{d+1} \sum_{J=0}^{d} \left[G_{\varphi_1} \left(\sum_{r^*=0}^{r_1} \hat{f}(\varsigma), \ \sum_{r^*=0}^{r_1} \hat{g}(\varsigma), \ \sum_{r^*=0}^{r_1} \hat{\theta}_1(\varsigma), \ \sum_{I=0}^{r_1} \hat{\varphi}_1(\varsigma) \right)_{\varsigma = J\delta\varsigma} \right]^2, \tag{26}$$

$$\hat{E}_{r_1}^{*N} = \frac{1}{d+1} \sum_{J=0}^{d} \left[G_N \left(\sum_{r^*=0}^{r_1} \hat{f}(\varsigma), \ \sum_{r^*=0}^{r_1} \hat{g}(\varsigma), \ \sum_{r^*=0}^{r_1} \hat{\varphi}_1(\varsigma), \ \sum_{r^*=0}^{r_1} \hat{N}(\varsigma) \right)_{\varsigma = J\delta\varsigma} \right]^2. \tag{27}$$

In view of Liao's exceptional contributions,[46]

$$\hat{E}_{r_1}^{*t} = \hat{E}_{r_1}^{*f} + \hat{E}_{r_1}^{*g} + \hat{E}_{r_1}^{*\theta_1} + \hat{E}_{r_1}^{*\varphi_1} + \hat{E}_{r_1}^{*N}, \tag{28}$$

where $\hat{E}_{r_1}^{*t}$ attitudes for total squared residual errors.

A. Convergence analysis

Theoretical interpretation for velocity, temperature, concentration, and density of motile microorganisms is presented. An optimal homotopic solution is achieved for the overriding resulting physical system. Table I is prepared for the convergence and reliability of the homotopic procedure. It presents that error diminishes for the required solutions by augmenting the order of approximations.

VI. PARAMETRIC ANALYSIS OF ACHIEVED SOLUTIONS AND PHYSICAL INTERPRETATION

This section focuses on the analysis of effects of active physical parameters on velocity, temperature, concentration, and density of motile microorganism profiles graphically by engaging OHAM. From Figs. 2–11, the influence of various physical parameters such as the Casson fluid parameter(χ), power index (n), Hartman number (M), mixed convection parameter (π_T), Prandtl number (Pr_∞), Brownian motion parameter (N_B), thermophoresis motion parameter (N_T), microorganism concentration difference parameter (Ω_1), Schmidt number(Sc_∞), bioconvection Peclet number (P_E), and bioconvection Lewis number (L_B) is discussed. Tables II and III present the comparative analysis of the applied scheme to the reduced problem available in the literature, and by noticing the results, excellent agreement is found.
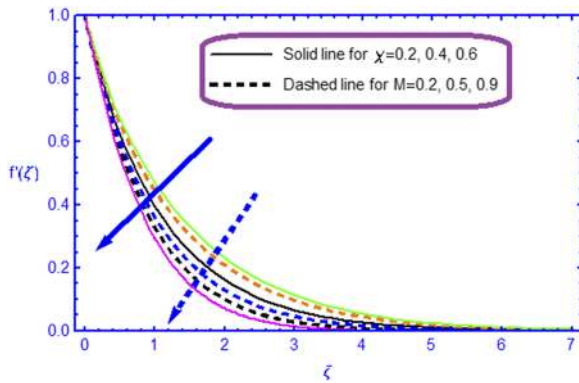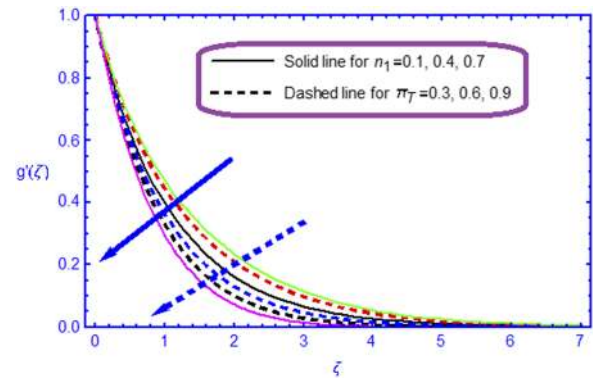
FIG. 2. Variation of χ and M on $f'(\zeta)$.

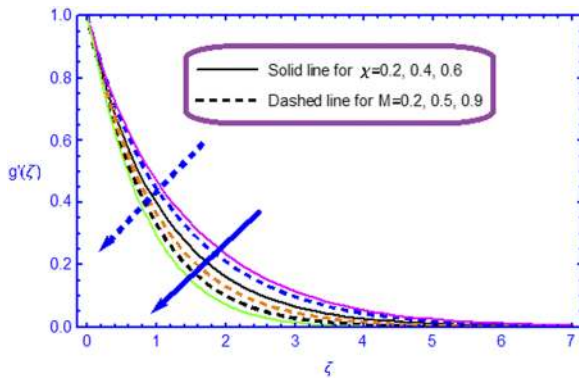**FIG. 5**. Variation of n_1 and π_T on $g'(\zeta)$.

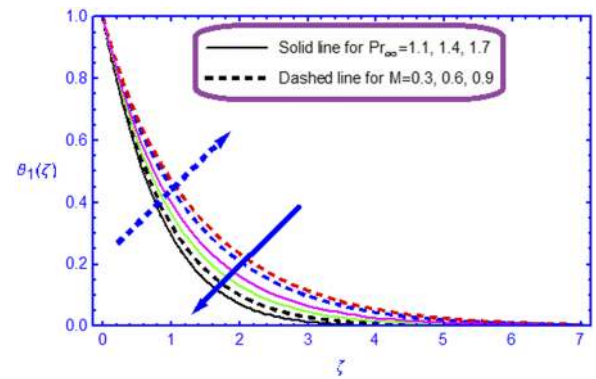
FIG. 3. Effect of χ and M on $g'(\zeta)$.

FIG. 6. Influence of Pr_∞ and M on $\theta_1(\zeta)$.

Figures 2 and 3 demonstrate the effect of the Casson fluid parameter (χ) and Hartman number(M) on velocity profiles $f'(\zeta)$ and $g'(\zeta)$, respectively. It is indicated that a large value of Casson fluid parameter declines both the momentum and thermal thickness between the boundary layers. The higher viscous forces on the flow

generated due to the rising parameter (χ) ascribed to this cause we can see decrement in the velocity profiles. Similarly, for increasing Hartman number (M), a resistive Lorentz force is produced and that resistive force is accountable for the decline of velocity profiles $f'(\zeta)$ and $g'(\zeta)$. The behavior of velocity profiles $g'(\zeta)$ and $f'(\zeta)$ for several
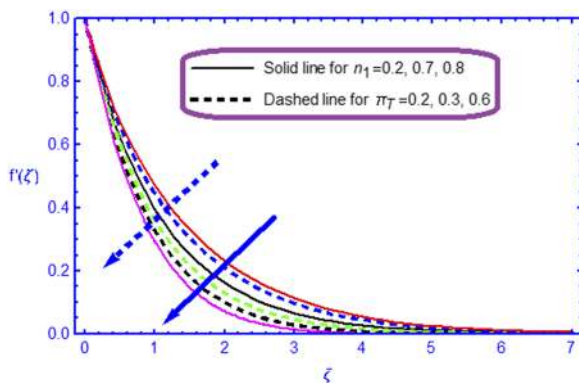

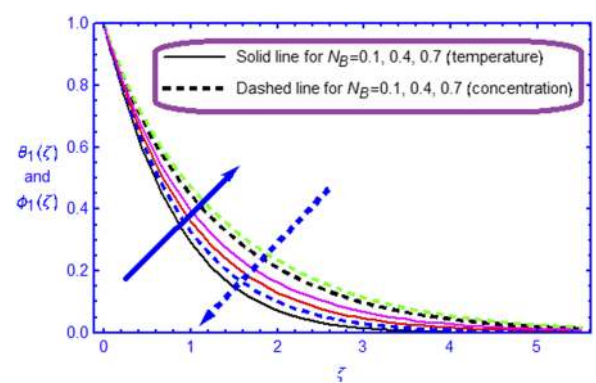**FIG. 4**. Inspiration of n_1 and π_T $f'(\zeta)$.

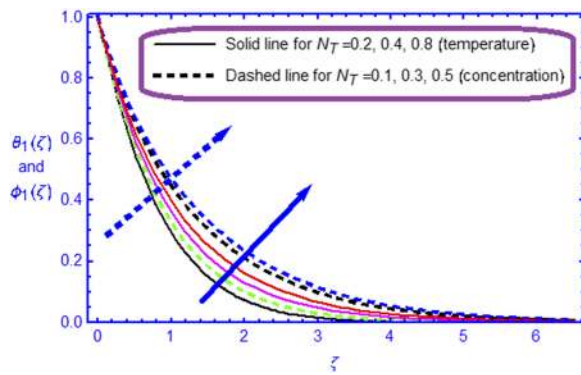**FIG. 7**. Effect of N_B on $\theta_1(\zeta)$ and $\varphi_1(\zeta)$.

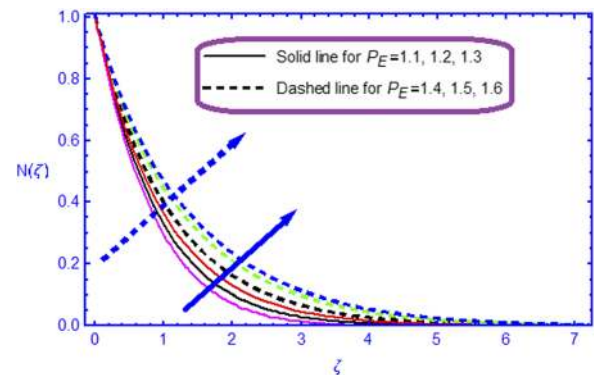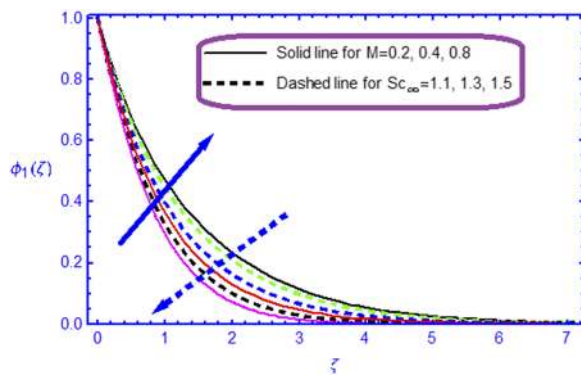**FIG. 8**. Behavior of N_T on $\theta_1(\zeta)$ and $\varphi_1(\zeta)$.

FIG. 9. Variation of M and Sc_∞ on $\varphi_1(\zeta)$.

values of power index (n_1) and mixed convection parameter (π_T) is presented in Figs. 4 and 5, respectively. It is noticed that variations of the power index (n_1) and mixed convection parameter (π_T) have reverse behavior with velocities profiles. Large values of (n_1) increase the nonlinearity of the surface between the fluid layers, and this decreases resistive force which tends to decrease the velocities. It also
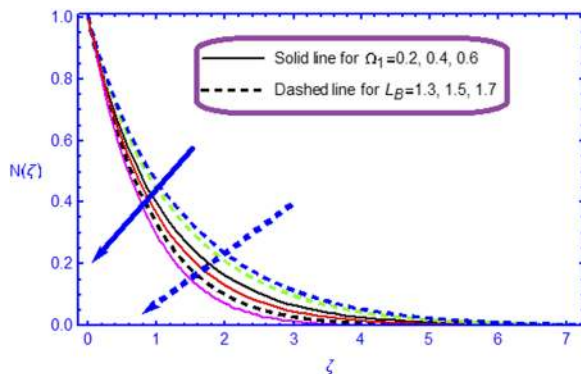

FIG. 10. Influence of Ω_1 and L_B on $N(\zeta)$.
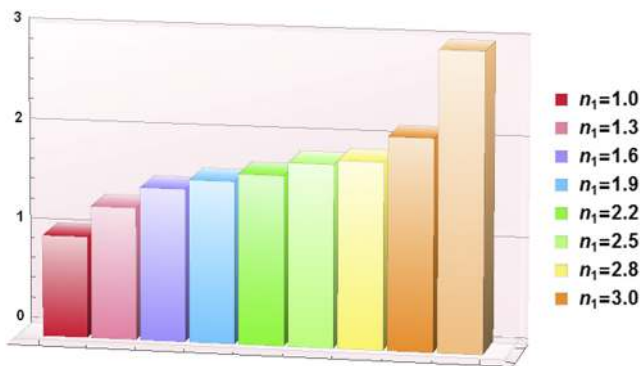

FIG. 11. Variation of P_E on $N(\zeta)$.

shows that the velocity profiles decrease for several values of mixed convection parameters (π_T). As (π_T) increases, it is inversely related to the Reynolds number, the buoyancy force decreases, and hence the fluid flow deaccelerates. Figure 6 exhibits that the temperature profile $\theta_1(\zeta)$ is enhanced with the variation of the Hartman number (M) and declined with the variation of the Prandtl number (Pr_∞). As expected, increasing values of (Pr_∞) reduce the fluid temperature $\theta_1(\zeta)$ as well as decrease thermal boundary layer thickness. It is to be observed that large values of (Pr_∞) decrease $\theta_1(\zeta)$ significantly and the boundary layer is squeezed near to the wall. The justification of this phenomenon is that the Prandtl number is interpreted as the ratio of the momentum diffusion to thermal diffusion. In the case of an increment in (M), the temperature profile enhances. It is physically justified due to Joule heating; with joule heating, the nanoparticle motion increases, which enhances the temperature boundary layer. The opposite nature of temperature and concentration profile is noticed for large values of the Brownian motion parameter (N_B), as shown in Fig. 7. It is a well known fact that the Brownian motion is the process of diffusion. The high-rise diffusivity implies higher temperature, and as a consequence, thermal conductivity also rises and the effect of Brownian motion in nanofluid is due to the nanoparticles. In addition to this fact, it enhances the nanoparticle kinetic energy which is mainly due to the increment in (N_B); as a result, the temperature of nanofluid rises. The concentration profile $\varphi_1(\zeta)$ decreases with an increase in (N_B) due to a rise in the kinetic energy of nanoparticles. The temperature profile $\theta_1(\zeta)$ and concentration profile $\varphi_1(\zeta)$ show similar increasing behavior for large values of the thermophoresis parameter (N_T), as seen in Fig. 8. In the process of thermophoresis motion, heated particles move away from the hottest place to the coldest region. For that fact, fluid temperature $\theta_1(\zeta)$ and concentration profile $\varphi_1(\zeta)$ enhance. Figure 9 demonstrates the performance of the Hartman number (M) and Schmidt number(Sc_∞) on the concentration profile $\varphi_1(\zeta)$. $\varphi_1(\zeta)$ considerably rises with an increase in (M). It is mainly the repercussion of thermophoresis boundary condition and Joule heating. With an increment in (Sc_∞), the concentration profile $\varphi_1(\zeta)$ diminishes. With an increasing in (Sc_∞), there is a decrement in the molecular diffusivity of nanoparticles; as a result, concentration boundary layer thickness reduces. Because of this fact, $\varphi_1(\zeta)$ decays with increasing (Sc_∞). The effect of the concentration difference parameter (Ω_1) and bioconvective Lewis number (L_B) on the concentration of microorganisms

TABLE II. Numerical data of $\left(1 + \frac{1}{\chi}\right) f''(0)$ and $\left(1 + \frac{1}{\chi}\right) g''(0)$ for different values of n_1, A by setting $\chi = \infty$, $\pi_T = B_T = B_C = 0 = M$.
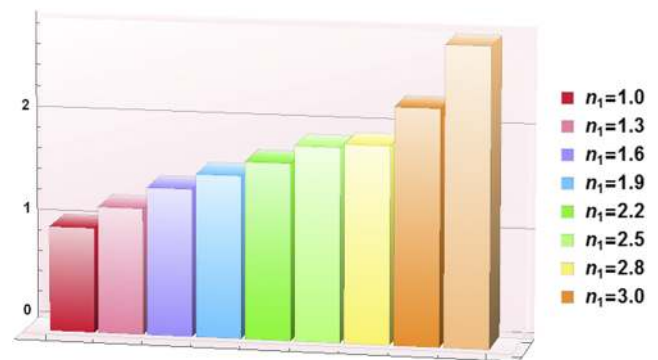
n_1	A	$\left(1 + \frac{1}{\chi}\right)f''(0)$ [48,49]		$\left(1 + \frac{1}{\chi}\right)g''(0)$ [48,49]		$\left(1 + \frac{1}{\chi}\right)f''(0)$	$\left(1 + \frac{1}{\chi}\right)g''(0)$
		Shooting	bvp5c	Shooting	bvp5c	Present	Present
1	0	−1	−1	0	0	−1	0
...	0.5	−1.224 745	1.224 742	−0.612 372	−0.612 371	−1.224 745	−0.612 371
...	1	−1.414 214	−1.414 214	−1.414 214	−1.414 214	−1.414 214	−1.414 214
3	0	−1.624 356	−1.624 356	0	0	−1.624 356	0
...	0.5	−1.989 422	−1.989 422	−0.994 711	−0.994 711	−1.989 421	−0.994 710
...	1	−2.297 186	−2.297 182	−2.297 186	−2.297 182	−2.297 186	−2.297 186

TABLE III. Numerical values of the Nusselt number $Nu = -\theta_1'(0)\,(1 + \delta_1\theta_1(0))$ for numerous values of A, n_1, Pr_∞ when $M = \pi_T = 0 = B_T = B_C = N_T = \delta_1$.

n_1	Pr_∞	A	Nu[48] shooting	Nu[48] bvp5c	Nu (present)
1.0	0.7	0.0	0.793 668	0.793 668	0.793 668
...	...	0.5	0.972 033	0.972 029	0.972 031
...	...	1.0	1.122 406	1.122 321	1.122 404
...	1.0	0.0	1.000 000	0.999 990	1.000 000
...	...	0.5	1.224 745	1.224 742	1.224 745
...	...	1.0	1.414 214	1.414 214	1.414 214
...	7.0	0.0	3.072 250	3.072 251	3.072 250
...	...	0.5	3.762 723	3.762 724	3.762 722
...	...	1.0	4.344 818	4.344 779	4.344 818
3.0	0.7	0.0	1.292 193	1.292 194	1.292 193
...	...	0.5	1.582 607	1.582 607	1.582 605
...	...	1.0	1.827 437	1.827 427	1.827 437
...	1.0	0.0	1.624 356	1.624 356	1.624 356
...	...	0.5	1.928 942 2	1.989 422	1.989 422
...	...	1.0	2.297 186	2.297 182	2.297 186
...	7.0	0.0	4.968 777	4.968 777	4.968 777
...	...	0.5	6.085 484	6.085 485	6.085 484
...	...	1.0	7.026 912	7.026 913	7.026 911

FIG. 13. Variation of dimensionless stress y-component against n_1.

$N(\zeta)$ is strategized in Fig. 10. For enhancing (Ω_1), this increases the concentration for ambient fluid but decreases the surface concentration of microorganisms. For increasing values of (L_B), the diffusivity of swimming microorganisms is diminished; thus, the local concentration of microorganisms has been decreased. Figure 11 illustrates the variation of the concentration of microorganisms $N(\zeta)$ for various values of Peclet numbers (P_E). $N(\zeta)$ enhances as we increase the Peclet number (P_E), which shows that the buoyancy parameter is inaugurated to be more assured for a fluid with greater values of (P_E). Dimensionless stresses are plotted through a bar chart as presented in Figs. 12 and 13 against varying values of indexed number. It presents that stresses grows as it boosts.

VII. CONCLUDING COMMENTS AND KEY OBSERVATIONS OF PRESENT DELIBERATION

Bioconvective flow of a Casson fluid with heat and mass transfer over a bidirectional nonlinear stretched surface having a variable magnetic field, thermal conductivity, and mass diffusion coefficient is inspected. Boundary layer equations are handled analytically via the optimal homotopic algorithm. The effect of influential variables on computed solution is displayed through graphs and tables. The key findings of the present experiment is listed as follows:

- Nondimensional fluid velocity decreased by escalating the values of the magnetic parameter, indexed number, mixed convection parameter, and Casson fluid parameter.

FIG. 12. Variation of dimensionless stress x-component against n_1.

- Fluid temperature and associated layer thickness increased by mounting the values of the magnetic parameter and decreased for greater values of Prandtl numbers.
- Dimensionless stresses grow by mounting the values of the indexed number, which presents the direct relation.
- Brownian motion parameter has the opposite impact on fluid temperature and concentration profiles.
- Escalating values of the thermophoresis parameter upsurges the fluid temperature and concentration and related layer thickness.
- An increase in Schmidt number decreases the fluid concentration, whereas it grows for mounting values of the magnetic parameter.
- Motile density profile decreased for mounting values of the concentration difference parameter and Lewis number, whereas the Peclet number boosted it.

REFERENCES

[1] M. S. Aghighi, A. Ammar, C. Metivier, and M. Gharagozlu, "Rayleigh-Bénard convection of Casson fluids," Int. J. Therm. Sci. **127**, 79–90 (2018).

[2] J. Raza, "Thermal radiation and slip effects on magnetohydrodynamic (MHD) stagnation point flow of Casson fluid over a convective stretching sheet," Propul. Power Res. **8**, 138 (2019).

[3] S. E. Ahmed, M. A. Mansour, A. Mahdy, and S. S. Mohamed, "Entropy generation due to double diffusive convective flow of Casson fluids over nonlinearity stretching sheets with slip conditions," Eng. Sci. Technol., Int. J. **20**(6), 1553–1562 (2017).

[4] F. Mabood and K. Das, "Outlining the impact of melting on MHD Casson fluid flow past a stretching sheet in a porous medium with radiation," Heliyon **5**(2), e01216 (2019).

[5] Z. Shah, A. Dawar, I. Khan, S. Islam, D. L. C. Ching, and A. Z. Khan, "Cattaneo-Christov model for electrical magnetite micropoler Casson ferrofluid over a stretching/shrinking sheet using effective thermal conductivity model," Case Stud. Therm. Eng. **13**, 100352 (2019).

[6] S. T. Mohyud-Din, M. Usman, W. Wang, and M. Hamid, "A study of heat transfer analysis for squeezing flow of a Casson fluid via differential transform method," Neural Comput. Appl. **30**(10), 3253–3264 (2018).

[7] A. Mehmood, M. Usman, and B. Weigand, "Heat and mass transfer phenomena due to a rotating non-isothermal wavy disk," Int. J. Heat Mass Transfer **129**, 96–102 (2019).

[8] X. Y. Sun, Y. J. Dai, T. S. Ge, Y. Zhao, and R. Z. Wang, "Heat and mass transfer comparisons of desiccant coated microchannel and fin-and-tube heat exchangers," Appl. Therm. Eng. **150**, 1159–1167 (2019).

[9] X. Zhang, J. Wu, and Z. Li, "Irreversibility characterization and analysis of coupled heat and mass transfer processes in an absorption system," Int. J. Heat Mass Transfer **133**, 1121–1133 (2019).

[10] J. Liu, X. Liu, and T. Zhang, "Analytical solution of heat and mass transfer process in internally cooled liquid desiccant dehumidifiers using refrigerant as cooling medium," Energy Build. **190**, 1–14 (2019).

[11] N. Akmal, M. Sagheer, S. Hussain, and A. Kamran, "Investigation of free convection in micropolar nanofluid with induced magnetic field," Eur. Phys. J. Plus **134**(5), 235 (2019).

[12] M. Hamid, M. Usman, Z. H. Khan, W. Wang, and R. Ahmad, "Dual solutions and stability analysis of flow and heat transfer of Casson fluid on a stretching sheet with convective boundary condition," Phys. Lett. A **383**, 2400 (2019).

[13] V. J. Inglezakis, M. M. Fyrillas, and J. Park, "Variable diffusivity homogeneous surface diffusion model and analysis of merits and fallacies of simplified adsorption kinetics equations," J. Hazard. Mater. **367**, 224 (2018).

[14] M. Hamid, M. Usman, T. Zubair, R. U. Haq, and W. Wang, "Shape effects of MoS_2 nanoparticles on rotating flow of nanofluid along a stretching surface with variable thermal conductivity: A Galerkin approach," Int. J. Heat Mass Transfer **124**, 706–714 (2018).

[15] I. V. Stepanova, "Group analysis of variable coefficients heat and mass transfer equations with power nonlinearity of thermal diffusivity," Appl. Math. Comput. **343**, 57–66 (2019).

[16] M. Aouadi, A. R. E. Dhaba, and A. F. Ghaleb, "Nonlinear theory for thermoelastic solids with mass diffusion," Eur. J. Mech. A: Solids **70**, 267–279 (2018).

[17] M. Nawaz, R. Naz, and M. Awais, "Magnetohydrodynamic axisymmetric flow of Casson fluid with variable thermal conductivity and free stream," Alexandria Eng. J. **57**(3), 2043–2050 (2018).

[18] J. Ahmed, M. Khan, and L. Ahmad, "MHD swirling flow and heat transfer in Maxwell fluid driven by two coaxially rotating disks with variable thermal conductivity," Chin. J. Phys. **60**, 22 (2019).

[19] M. Bilal, M. Sagheer, and S. Hussain, "Numerical study of magnetohydrodynamics and thermal radiation on Williamson nanofluid flow over a stretching cylinder with variable thermal conductivity," Alexandria Eng. J. **57**(4), 3281–3289 (2018).

[20] A. Hamid and M. Khan, "Unsteady mixed convective flow of Williamson nanofluid with heat transfer in the presence of variable thermal conductivity and magnetic field," J. Mol. Liq. **260**, 436–446 (2018).

[21] N. Sandeep and I. L. Animasaun, "Heat transfer in wall jet flow of magnetic-nanofluids with variable magnetic field," Alexandria Eng. J. **56**(2), 263–269 (2017).

[22] A. Kamran, S. Hussain, and M. Sagheer, "Impact of induced magnetic field on free convective flow of kerosene/water based single and multiwalled carbon nanotubes," AIP Adv. **8**(10), 105130 (2018).

[23] M. Sheikholeslami, S. A. M. Mehryan, A. Shafee, and M. A. Sheremet, "Variable magnetic forces impact on magnetizable hybrid nanofluid heat transfer through a circular cavity," J. Mol. Liq. **277**, 388–396 (2019).

[24] M. Izadi, R. Mohebbi, A. A. Delouei, and H. Sajjadi, "Natural convection of a magnetizable hybrid nanofluid inside a porous enclosure subjected to two variable magnetic fields," Int. J. Mech. Sci. **151**, 154–169 (2019).

[25] C. Ciobotaru and I. Gruia, "Main factors affecting the appearance of M-effect in variable magnetic field," Vacuum **167**, 500 (2018).

[26] M. Hatami, J. Zhou, J. Geng, and D. Jing, "Variable magnetic field (VMF) effect on the heat transfer of a half-annulus cavity filled by Fe_3O_4-water nanofluid under constant heat flux," J. Magn. Magn. Mater. **451**, 173–182 (2018).

[27] J. R. Platt, "Bioconvection patterns in cultures of free-swimming organisms," Science **133**, 1766–1767 (1961).

[28] S. Mosayebidorcheh, M. A. Tahavori, T. Mosayebidorcheh, and D. D. Ganji, "Analysis of nano-bioconvection flow containing both nanoparticles and gyrotactic microorganisms in a horizontal channel using modified least square method (MLSM)," J. Mol. Liq. **227**, 356–365 (2017).

[29] M. Khan, M. Irfan, and W. A. Khan, "Impact of nonlinear thermal radiation and gyrotactic microorganisms on the Magneto-Burgers nanofluid," Int. J. Mech. Sci. **130**, 375–382 (2017).

[30] Z. Iqbal, Z. Mehmood, and E. N. Maraj, "Oblique transport of gyrotactic microorganisms and bioconvection nanoparticles with convective mass flux," Physica E **88**, 265–271 (2017).

[31] S. Qayyum, M. Imtiaz, A. Alsaedi, and T. Hayat, "Analysis of radiation in a suspension of nanoparticles and gyrotactic microorganism for rotating disk of variable thickness," Chin. J. Phys. **56**(5), 2404–2423 (2018).

[32]M. Usman, M. Hamid, and M. M. Rashidi, "Gegenbauer wavelets collocation-based scheme to explore the solution of free bio-convection of nanofluid in 3D nearby stagnation point," Neural Comput. Appl. **31**, 8003–8019 (2018).

[33]V. Marinca, N. Herişanu, C. Bota, and B. Marinca, "An optimal homotopy asymptotic method applied to the steady flow of a fourth-grade fluid past a porous plate," Appl. Math. Lett. **22**(2), 245–251 (2009).

[34]K. V. Prasad, K. Vajravelu, H. Vaidya, N. Z. Basha, and V. Umesh, "Thermal and species concentration of MHD Casson fluid at a vertical sheet in the presence variable fluid properties," Ain Shams Eng. J. **9**(4), 1763–1779 (2018).

[35]T. Fan and X. You, "Optimal homotopy analysis method for nonlinear differential equations in the boundary layer," Numer. Algorithms **62**(2), 337–354 (2013).

[36]M. Awais, S. E. Awan, K. Iqbal, Z. A. Khan, and M. A. Z. Raja, "Hydromagnetic mixed convective flow over a wall with variable thickness and Cattaneo-Christov heat flux model: OHAM analysis," Results Phys. **8**, 621–627 (2018).

[37]M. Awais, S. Saleem, T. Hayat, and S. Irum, "Hydromagnetic couple-stress nanofluid flow over a moving convective wall: OHAM analysis," Acta Astronaut. **129**, 271–276 (2016).

[38]M. Sheikholeslami, S. A. Shehzad, and Z. Li, "Water based nanofluid free convection heat transfer in a three dimensional porous cavity with hot sphere obstacle in existence of Lorentz forces," Int. J. Heat Mass Transfer. **125**, 375–386 (2018).

[39]M. Sheikholeslami, S. A. Shehzad, F. M. Abbasi, and Z. Li, "Nanofluid flow and forced convection heat transfer due to Lorentz forces in a porous lid driven cubic enclosure with hot obstacle," Comput. Methods Appl. Mech. Eng. **338**, 491–505 (2018).

[40]M. Sheikholeslami and A. Zeeshan, "Analysis of flow and heat transfer in water based nanofluid due to magnetic field in a porous enclosure with constant heat flux using CVFEM," Comput. Methods Appl. Mech. Eng. **320**, 68–81 (2017).

[41]M. Sheikholeslami, M. Jafaryar, and Z. Li, "Second law analysis for nanofluid turbulent flow inside a circular duct in presence of twisted tape turbulators," J. Mol. Liq. **263**, 489–500 (2018).

[42]O. E. Alzahrani, Z. Shah, W. Alghamdi, and M. Zaka Ullah, "Darcy-Forchheimer radiative flow of micropoler CNT nanofluid in rotating frame with convective heat generation/consumption," Processes **7**, 666 (2019).

[43]M. Hamid, M. Usman, Z. H. Khan, R. U. Haq, and W. Wang, "Numerical study of unsteady MHD flow of Williamson nanofluid in a permeable channel with heat source/sink and thermal radiation," Eur. Phys. J. Plus **133**(12), 527 (2018).

[44]Z. Shah, H. Babazadeh, P. Kumam, A. Shafee, and P. Thounthong, "Numerical simulation of magnetohydrodynamic nanofluids under the influence of shape factor and thermal transport in a porous media using CVFEM," Front. Phys. **7**, 164 (2019).

[45]S. J. Liao, *Homotopy Analysis Method in Nonlinear Differential Equations* (Springer and Higher Education Press, Heidelberg, 2012).

[46]S. J. Liao, "An optimal homotopy analysis approach for strongly nonlinear differential equations," Commun. Nonlinear Sci. Numer. Simul. **15**, 2003–2016 (2010).

[47]S. Bilal, M. Sohail, R. Naz, and M. Y. Malik, "Dynamical and optimal procedure to analyse the exhibition of physical attribute imparted by Sutterby Magneto nano fluid in Darcy medium yield by axially stretched cylinder," Can. J. Phys. **97**, 579 (2019).

[48]J. A. Khan, M. Mustafa, T. Hayat, and A. Alsaedi, "Three-dimensional flow of nanofluid over a non-linearly stretching sheet: An application to solar energy," Int. J. Heat Mass Transfer **86**, 158–164 (2015).

[49]J. A. Khan, M. Mustafa, T. Hayat, and A. Alsaedi, "On three-dimensional flow and heat transfer over a non-linearly stretching sheet: Analytical and numerical solutions," PLoS One **9**(9), e107287 (2014).

[50]A. Kamran, S. Hussain, M. Sagheer, and N. Akmal, "A numerical study of magnetohydrodynamics flow in Casson nanofluid combined with Joule heating and slip boundary conditions," Results Phys. **7**, 3037–3048 (2017).

[51]M. Sohail, R. Naz, and S. I. Abdelsalam, "Application of non-Fourier double diffusions theories to the boundary-layer flow of a yield stress exhibiting fluid model," Physica A **537**, 122753 (2020).